HYSTERESIS PHENOMENA IN THE RESPONSE OF GEOMAGNETIC ACTIVITY AND COSMIC RAY PARAMETERS TO VARIATIONS IN THE INTERPLANETARY MEDIUM DURING A MAGNETIC STORM

O.A. Danilova
Pushkov Institute of Terrestrial Magnetism, Ionosphere, and Radio Wave Propagation, St. Petersburg Branch, RAS, St. Petersburg, Russia, md1555@mail.ru

N.G. Ptitsyna
Pushkov Institute of Terrestrial Magnetism, Ionosphere, and Radio Wave Propagation, St. Petersburg Branch, RAS, St. Petersburg, Russia, nataliaptitsyna@yahoo.com

V.E. Sdobnov
Institute of Solar-Terrestrial Physics SB RAS, Irkutsk, Russia, sdobnov@iszf.irk.ru

Abstract. The dynamics of the intensity of cosmic rays is known to be different on the ascending and descending branches of the 11-year solar cycle, i.e., hysteresis phenomena are observed. Recently, it has been obtained that at shorter intervals on the scale of magnetic storms there are also signs of hysteresis in dependences of cosmic ray cutoff rigidities R (geomagnetic thresholds) on heliosphere and geosphere parameters. R is the rigidity below which a particle flux is cut off due to geomagnetic shielding. In this paper, we have analyzed the dependence of the geomagnetic storm index Dst and the variation of the ΔR thresholds on interplanetary magnetic field (IMF) and solar wind (SW) parameters during the two-step magnetic storm on September 7–8, 2017. We have found hysteresis phenomena in the following paired series: (1) dependences of Dst on SW and IMF parameters, and (2) dependences of ΔR on SW and IMF parameters. We have established that the dependence curves in the storm descending phase (main phase) and ascending phase (recovery phase) do not coincide — hysteresis loops are formed. A specific feature of the storm under study is the second lowering of Dst in the recovery phase. The hysteresis pattern reflects this specific storm dynamics, forming two hysteresis loops in response to the two Dst drops.

Keywords: cosmic rays, geomagnetic threshold, cosmic ray cutoff rigidities, supersubstorm, interplanetary magnetic field, geomagnetic activity.

INTRODUCTION

Cosmic rays (CRs) are fluxes of charged energetic particles penetrating into interplanetary space. They come from both near solar space and distant galactic space. Penetration of CRs into the magnetosphere is controlled by the geomagnetic threshold or the geomagnetic cutoff rigidity R, below which a particle flux is cut off due to geomagnetic shielding. At the magnetic poles, R is minimal (almost zero), and in the vicinity of the equator it increases to vertical R~15 GV. During geomagnetic storms, geomagnetic shielding decreases due to a decrease in the field inside the magnetosphere because of the formation of global current systems — ring current, magnetopause currents, magnetotail and field-aligned high-latitude currents. As a result, cosmic particles can penetrate to lower latitudes.

Variations in solar activity and galactic CR intensity exhibit hysteresis effects: the dynamics of CR intensity is different on the ascending and descending branches of the 11-year cycle. These effects on ten-year time scales were observed more than twenty years ago in [Mavromichalaki et al., 1998; Dorman et al., 2001; Kane, 2003]. The authors correlated the obtained hysteresis with the delay in the interplanetary processes, responsible for CR modulation, with respect to corresponding solar processes and solar wind (SW) parameters. It has recently been found that for

some CR characteristics, hysteresis effects can also be observed on shorter time scales of the order of the evolution time of a geomagnetic storm (several days). In [Ptitsyna et al., 2021; Danilova et al., 2023], it has been obtained that the dependences of ΔR variation on interplanetary magnetic field (IMF) and SW parameters during the magnetic storm descending phase (decrease in Dst, main phase) and the ascending one (recovery phase) do not coincide. This yields a loop diagram — a hysteresis loop. Besides, in [Kurazhkovskaya et al., 2021; Kurazhkovskaya, Kurazhkovsky, 2023], the presence of hysteresis was observed in the dependence of Dst on the SW plasma parameter β (this parameter is equal to the ratio of thermal pressure to magnetic one $β=NkT/(B^2/(8π))$) during the development of geomagnetic storms. From statistical analysis of the storms that occurred from 1964 to 2010, in [Kurazhkovskaya et al., 2021; Kurazhkovskaya, Kurazhkovsky, 2023] it has been found that the $Dst(β)$ dynamics during the storm main phase does not coincide with that during the recovery phase.

The effects of solar coronal mass ejections (CMEs), high-speed SW streams from coronal holes on Earth's magnetosphere cause geomagnetic disturbances of varying intensity. The strongest geomagnetic storms ($Dst<-100$ nT) are driven mainly by transient events: CMEs and related interplanetary structures (shock fronts, compression regions in front of interplanetary CMEs,

magnetic clouds, and magnetic pistons [Gosling, 1993; Yermolaev et al., 2010; Richardson, Cane, 2011; Obridko et al., 2013; Kilpua et al., 2017; Dremukhina et al., 2019]. In the case of interaction of CMEs with each other, as well as with other interplanetary features, complex structures with increased geoeffectiveness are formed in near-Earth space [Shen et al., 2018; Scolini et al., 2020].

A great scientific interest was aroused by a strong disturbance in near-Earth space and on Earth, which was generated by the passage of a similar structure and occurred on September 6–9, 2017. At that time there was increased solar activity, flares, CME, as well as magnetospheric and geomagnetic disturbances, which were accompanied by very strong substorms, a Forbush decrease in the CR intensity, and other features [Safargaleev, Tereshchenko, 2019; Scolini et al., 2020; Despirak et al., 2020; Hajra et al., 2020; Ptitsyna et al., 2023]. The severe geomagnetic storm on September 7–8, 2017 developed in two stages and on September 8 had two *Dst* minima: −142 at 01:00 UT and −124 nT at 17:00 UT.

The purpose of our work is to try to detect the hysteresis phenomena during the September 7–8, 2017 storm in paired series: 1) in the dependences of *Dst* on SW and IMF parameters; 2) in the dependences of ΔR on SW and IMF parameters. In addition, we intend to examine features of hysteresis formed during this complex, two-step storm.

1. METHODS AND DATA

Geomagnetic cutoff rigidities/geomagnetic thresholds have been calculated by two methods [Ptitsyna et al., 2023]. The first method involves calculating vertical effective cutoff rigidities R_{ef} by numerically integrating trajectories of charged particles in the model geomagnetic field [McCracken et al., 1962]. We have used the Tsyganenko magnetospheric magnetic field model Ts01 [Tsyganenko, 2002a, b; Tsyganenko et al., 2003], designed for disturbed conditions. This semi-empirical model is based on a database of satellite measurements of the magnetic field during 37 geomagnetic storms with *Dst*≤−65 nT. The main sources of the magnetic field of the Ts01 model are symmetric and partial ring currents, field-aligned Birkeland currents (regions 1 and 2), the magnetotail current system, and surface currents at the magnetopause. In Ts01, the *Dst* index, the SW density and velocity, as well as three IMF components are utilized as input parameters defining the effect of interplanetary conditions on the magnetosphere. These input parameters were taken from the OMNI database (Geopack–2008, [http://geo.phys.spbu.ru/~tsyganenko /modeling.html]). The variations in the geomagnetic thresholds ΔR_{ef} thus calculated are further referred to as model variations.

The second method of identifying variations in geomagnetic thresholds ΔR_{sgs} is the spectrographic global survey (SGS). The SGS method based on ground-based measurements of the CR intensity at the global network of stations provides information on CR variations caused by processes in interplanetary space, Earth's magnetosphere and atmosphere, which makes it possible to obtain variations in the differential rigidity spectrum of CRs at the boundary of the magnetosphere, pitch angular CR anisot-

ropy in interplanetary space, as well as variations in the planetary geomagnetic cutoff rigidity system at every instant [Kovalev et al., 2022]. In this case, the entire currently available complex of ground-based recording equipment is used (a worldwide network of neutron monitors located at any levels in Earth's atmosphere, ground-based and underground meson telescopes, etc.). The statistical error in determining ΔR_{sgs} in terms of the statistical accuracy of measurements at stations of the worldwide network does not exceed 0.05 GV in absolute value. The geomagnetic cutoff rigidity variations obtained by this method are further referred to as observed variations.

The cutoff rigidity variations ΔR_{ef} and ΔR_{sgs} were defined as differences between cutoff rigidities calculated every hour during the September 7–8, 2017 storm and cutoff rigidities in the quiet period before the storm. The daily average thresholds on September 6, 2017 were taken as quiet (*Dst*≈0).

The calculations have been made for the following stations: ESOI (Israel, 33.30° N, 35.80° E), AATB (Almaty, Kazakhstan, 43.20° N, 76.94° E), ROME (Rome, Italy, 41.90° N, 12.52° E), IRKT (Irkutsk, Russia, 52.47° N, 104.03° E), MOSC (Moscow, Russia, 55.47° N, 37.32° E), and KGSN (Kingston, Australia, 42.99° S, 147.29° E). The stations have been selected in such a way that under quiet conditions they covered the main range of threshold R_c affected by the geomagnetic field: ESOI — 10.29, ROME — 6.15, AATB — 5.94, IRKT — 3.17, MOSC — 2.11, KGSN — 1.88 GV. For 2017, we have employed the geomagnetic cutoff rigidity grid for 2020 and have calculated all results relative to 2020, using the program from the website [https://tools.izmiran.ru/cutoff/].

To calculate ΔR_{sgs}, we exploited data from the global network of CR stations [https://www.nmdb.eu]. Hourly SW (density *N*, velocity *V*, pressure *P*), IMF parameters (total field *B*, B_y, and B_z components), as well as the electric field azimuthal component E_y, the plasma parameter β, and *Dst* from the OMNI database on the website were used to calculate ΔR_{ef} and hysteresis diagrams [https://omniweb.gsfc.nasa.gov].

Plasma β is the ratio of plasma pressure to magnetic pressure; in the OMNI database, this parameter is calculated using the formula

$$\beta = \left(\frac{4.16T}{10^5} + 5.34 \right) \frac{N_p}{B^2},$$

where *T* is the temperature (K); N_p is the proton density (cm^{-3}); *B* is the total magnetic field (nT).

The electric field was calculated by the formula

$$E\left(\text{mV/m}\right) = -V\left(\text{km/s}\right) B_z\left(\text{nT}\right) \cdot 10^{-3}.$$

2. THE SEPTEMBER 7–8, 2017 STORM AND VARIATIONS IN GEOMAGNETIC THRESHOLDS

Figure 1 illustrates variations in ΔR_{ef} (*a*) and ΔR_{sgs} (*b*) on September 7–8, 2017. The thresholds ΔR_{sgs} and ΔR_{ef} are calculated by two methods for each of the six stations.
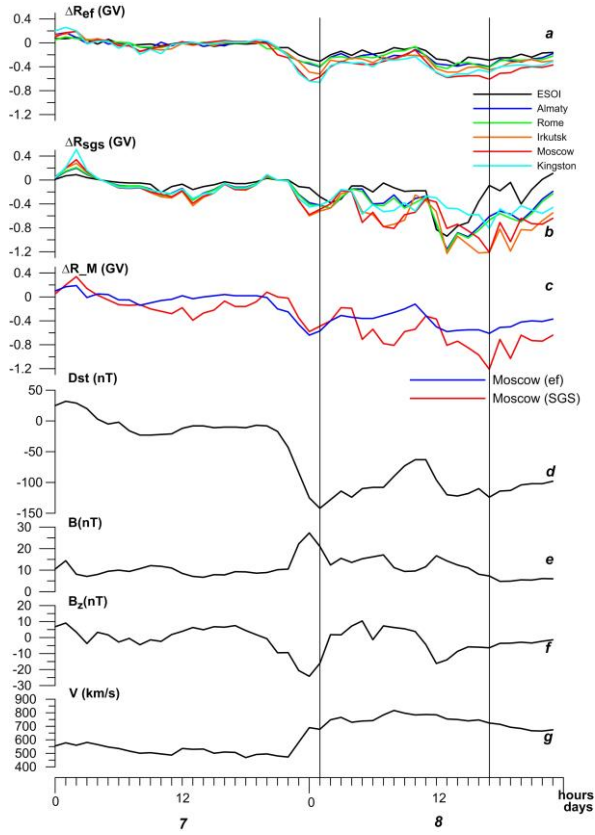
Figure 1. Variations in geomagnetic thresholds ΔR_{ef}, ΔR_{sgs}, and some IMF and SW parameters during the September 7–8, 2017 storm. Vertical lines indicate two decreases in *Dst*: Dst_{min1} and Dst_{min2}

For a more detailed comparison, the cutoff rigidity variations ΔR_{sgs} and ΔR_{ef} for the station Moscow (*c*) are plotted in a separate panel. Also shown is *Dst* (*d*), as well as some SW and IMF parameters characterizing the storm: *V*, IMF *B*, and B_z (*e–g*).

The magnetic storm is seen to reached a maximum $Dst_{min1} = -144$ nT on September 8 at ~01:00 UT. The storm main phase was accompanied by CME. A feature of the storm is the unsmooth behavior of the *Dst* time profile during the recovery phase with an additional decrease in Dst_{min2} associated with the arrival of another CME.

In general, the cutoff rigidity variations are seen to follow the *Dst* variations. This suggests that the ring current makes a major contribution to cutoff rigidity-variations.

Figure 1 shows that a maximum decrease in the model thresholds $\Delta R_{ef} = -0.66$ GV occurs during the first minimum Dst_{min1} at the end of the main phase. A maximum decrease in the observed thresholds $\Delta R_{sgs} = -1.21$ GV in the recovery phase during an additional decrease in $Dst_{min2} = -124$ nT.

Thus, there is a clearly noticeable difference in the response of observed ΔR_{sgs} and model ΔR_{ef} at midlatitudes (station Moscow).

3. HYSTERESIS PHENOMENA

3.1. Dependence of ΔR on *Dst*

We have examined the dependence of ΔR, calculated by the two methods, on the disturbance storm index *Dst*, using the station Moscow as an example. The dependences $\Delta R_{ef}(Dst)$ and $\Delta R_{sgs}(Dst)$ are plotted in Figure 2,

a, *b* respectively. The study is focused on the difference between the effects obtained during different storm phases. The dependences in the main (blue circles) and recovery (red circles) phases are shown. Note that the initial phase (several points grouped near *Dst*=0÷10 nT) is not highlighted in a separate color so as not to complicate the picture. The direction of the lead time of the processes coincides with the direction of the arrow.

Examine the dependence of ΔR_{ef} on *Dst* (panel *a*). During the storm, *Dst* varies cyclically (Figures 1, *d* and 2): in the main phase it decreases to Dst_{min1}, then in the recovery phase it increases, passing through an additional decrease in Dst_{min2}. Panel *a* shows that after the onset of the storm ΔR_{ef} decreases until the maximum of the storm Dst_{min1}, then the main phase is replaced by the recovery phase of the storm during which ΔR increases. Thus, the behavior of ΔR_{ef} repeats the behavior of *Dst*. Yet, the resulting dependence $\Delta R_{ef}(Dst)$ is ambiguous, it has a loop-like shape: the same value of ΔR_{ef} is obtained for different *Dst*. Panel *a* exhibits the dependence of ΔR_{ef} not only on the variable argument *Dst*, but also on the direction of the argument variation. The latter dependence is a sign of hysteresis. The descending and ascending curves of $\Delta R_{ef}(Dst)$ (the storm main and recovery phases) are seen to follow different trajectories,
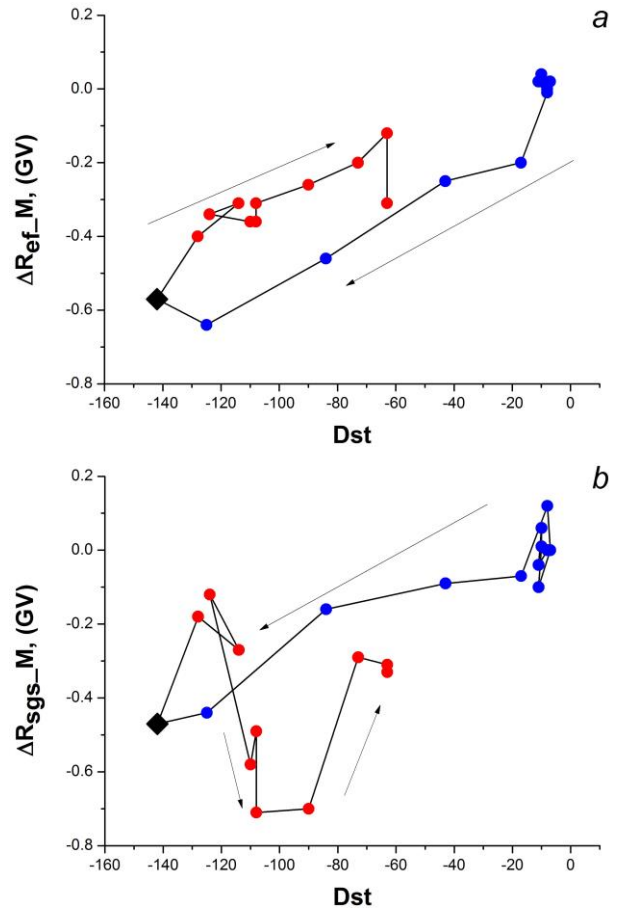

Figure 2. Dependences: $\Delta R_{ef}(Dst)$ (*a*); $\Delta R_{sgs}(Dst)$ (*b*) at the MOSC station. Blue circles indicate the main phase of the storm; the red ones, the recovery phase. The black diamond marks the maximum of the storm Dst_{min1}. The direction of the lead time of the processes coincides with the direction of the arrow

thereby producing a hysteresis loop, which reflects the response of ΔR_{ef} to a decrease in Dst_{min1} (a drop and then a rise in ΔR)

The dependence $\Delta R_{sgs}(Dst)$, shown in panel *b*, represents a more complex pattern. The $\Delta R_{sgs}(Dst)$ curve in the main phase to Dst_{min1} is similar to the $\Delta R_{sgs}(Dst)$ curve, but later on ΔR_{sgs} also reacts to the second decrease in Dst_{min2} during the storm recovery phase. The rise in ΔR_{sgs} is seen to be interrupted by a sharp drop after which the thresholds continue to increase again. As a result, the ascending curve of $\Delta R_{ef}(Dst)$ in the storm recovery phase contains a second open hysteresis loop as a response to Dst_{min2}.

Since a specific feature of the storm under study is an additional decrease in Dst_{min2} during the recovery phase, we can conclude that hysteresis of the observed ΔR_{sgs} values, by forming two loops (as a response to both decreases in Dst_{min1} and Dst_{min2}), better reflects the specifics of the storm than hysteresis of the model ΔR_{ef} values.

3.2. Dependence of *Dst* and ΔR on SW magnetic and electric parameters

In this section, we analyze data to identify hysteresis phenomena in the relationship of three paired series during the September 7–8, 2017 storm: 1) in the dependences of *Dst* on *B*, B_z, E_y, and β; 2) in the dependences of ΔR_{ef} on *B*, B_z, E_y, and β; 3) in the dependences of ΔR_{sgs} on the same interplanetary medium parameters. The result of the analysis for the station Moscow is presented in Figure 3 as diagrams of the dependence of *Dst*, ΔR_{ef}, and ΔR_{sgs} on each of the parameters considered. Panels *a–d* plot the dependence of *Dst* on *B*, B_z, E_y, and β; panels *e–h*, the dependence of model ΔR_{ef} on *B*, B_z, E_y, and β; panels *i–l*, the dependence of observed ΔR_{sgs} on the same parameters.
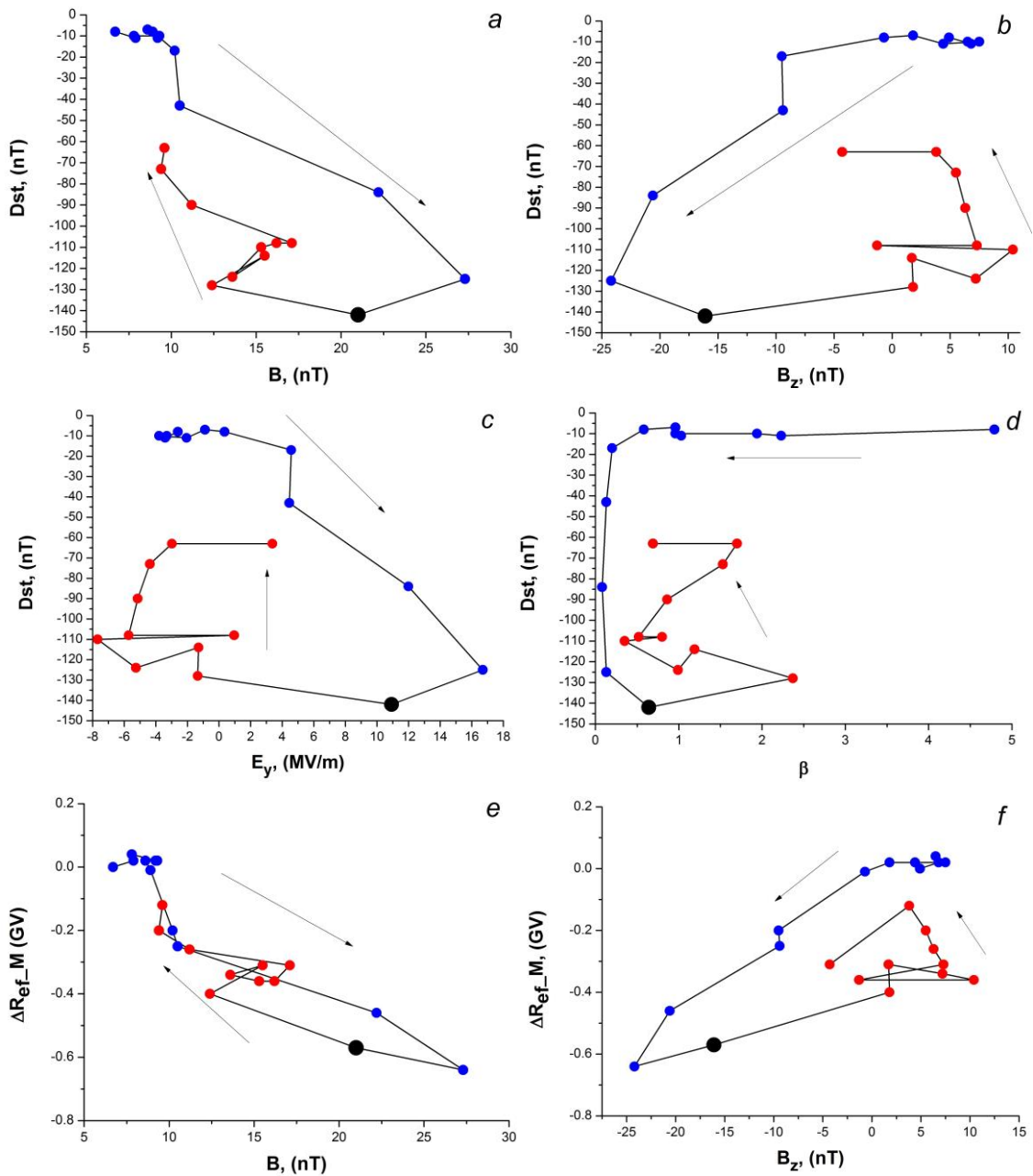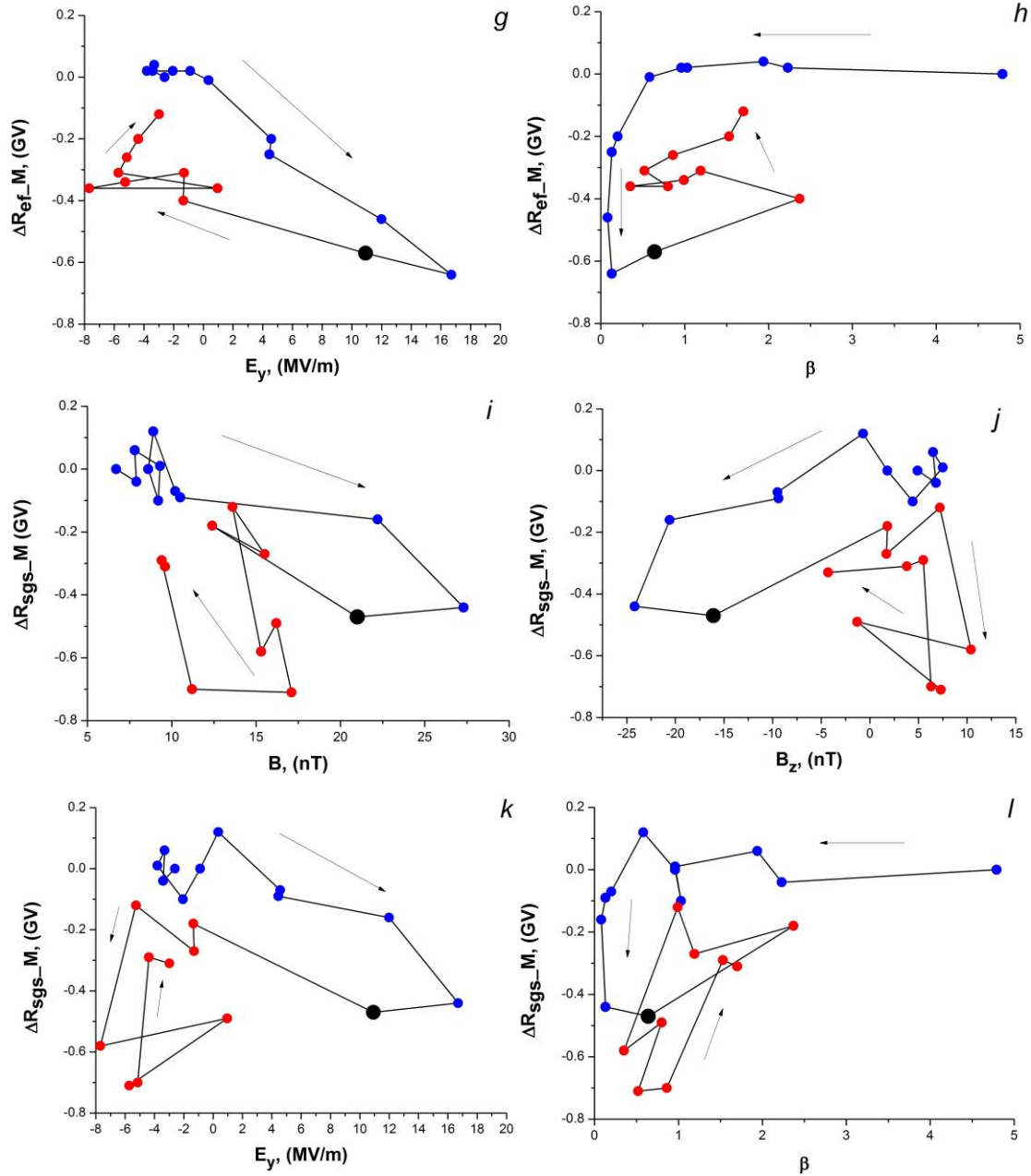
Figure 3. Hysteresis loops for the dependence of *Dst* and ΔR on parameters of the interplanetary magnetic and electric fields. Blue circles indicate the main phase; red ones, the recovery phase. The direction of the lead time of the processes coincides with the direction of the arrow

Analyze the evolution of *Dst* during the two-step storm depending on the SW magnetic and electric parameters (panels *a–d*). The dependence diagram *Dst*(*B*) (*a*) shows that *B* varies from values of the order of 5÷10 nT at the beginning of the storm, then during the main phase it increases to a maximum of 28 nT 1 hr before the storm maximum, decreasing afterward to 10 nT. Such a cyclic variation in *B* is accompanied by a cyclic variation in *Dst*: a drop during the main phase to *Dst*ₘᵢₙ₁ in the storm minimum and a subsequent rise. The *Dst*(*B*) curve exhibits a loop-like dependence since the descending portion of the curve (blue dots in the main phase) does not coincide with the portion of the curve in the ascending part (red dots in the recovery phase). Under cyclic variations in B_z, E_y, and β (*b–d*), similar hysteresis loops are seen to be formed for the dependences

Dst (B_z, E_y, β). Note that the ascending branches of the loops (the recovery phase) are not smooth, they are distorted by jumps in the SW magnetic and electric parameters at the second stage of the storm. One of the differences between the obtained hysteresis loops is that for *Dst*(*B*, E_y) the cycle is bypassed clockwise; and for *Dst*(B_z, β), counterclockwise. Furthermore, noteworthy is the different widths of the hysteresis loops obtained, which is likely related to the degree of symmetry/asymmetry of the initial process [Serensen et al., 1975; Atabekov, 2009].

Panels *e–h* also display signs of hysteresis in the dependence of ΔR_{sgs} on IMF and electric field parameters. The curve of the ΔR_{ef} dependence on one of the *B*, B_z, E_y, or β arguments as well as the diagrams of the left row of panels are characterized by two branches: de-

scending (initial and main phases of the storm) and ascending (recovery phase). The geomagnetic threshold decreases on the descending branch and increases on the ascending one. Panels *e–h* exhibit the ambiguity of the relationship between ΔR_{ef} and B, B_z, E_y, β. The trajectory of ΔR_{ef}, i.e. successive values that ΔR_{ef} takes in the dependence on B, B_z, E_y, and β in the main phase (blue symbols), does not significantly match the trajectory in the recovery phase (red symbols), with hysteresis loops being formed. For the dependences $\Delta R_{ef}(B, B_z, E_y, β)$, hysteresis loops are similar to the loops of $Dst(B, B_z, E_y, β)$. However, in this case there are two loops as a response to two decreases in Dst_{min1} and Dst_{min2}.

Panels *i–l* also show signs of hysteresis in the dependence of ΔR_{sgs} on IMF parameters. For $\Delta R_{sgs}(B, B_z, E_y, β)$, the descending portions of the loops (main phase) virtually fit the curves in the diagrams of the left and middle panels, i.e. Dst and $\Delta R_{ef}(B, B_z, E_y, β)$. Nonetheless, in the storm recovery phase (*i–l*) there are two loops as a response to two decreases in Dst_{min1} and Dst_{min2}.

In the dependences of ΔR_{ef} on the IMF parameters, a small additional loop is also seen as a response to the second decrease in Dst_{min2}, but it is much less pronounced.

3.3. Dependences of *Dst* and Δ*R* on SW dynamic parameters

Figure 4 illustrates the dependence of *Dst* (*a–c*), ΔR_{ef} (*d–f*), and ΔR_{sgs} (*g–i*) on the dynamic parameters *V*, *N*, and *P* for different SW magnetic and electric parameters during the storm.
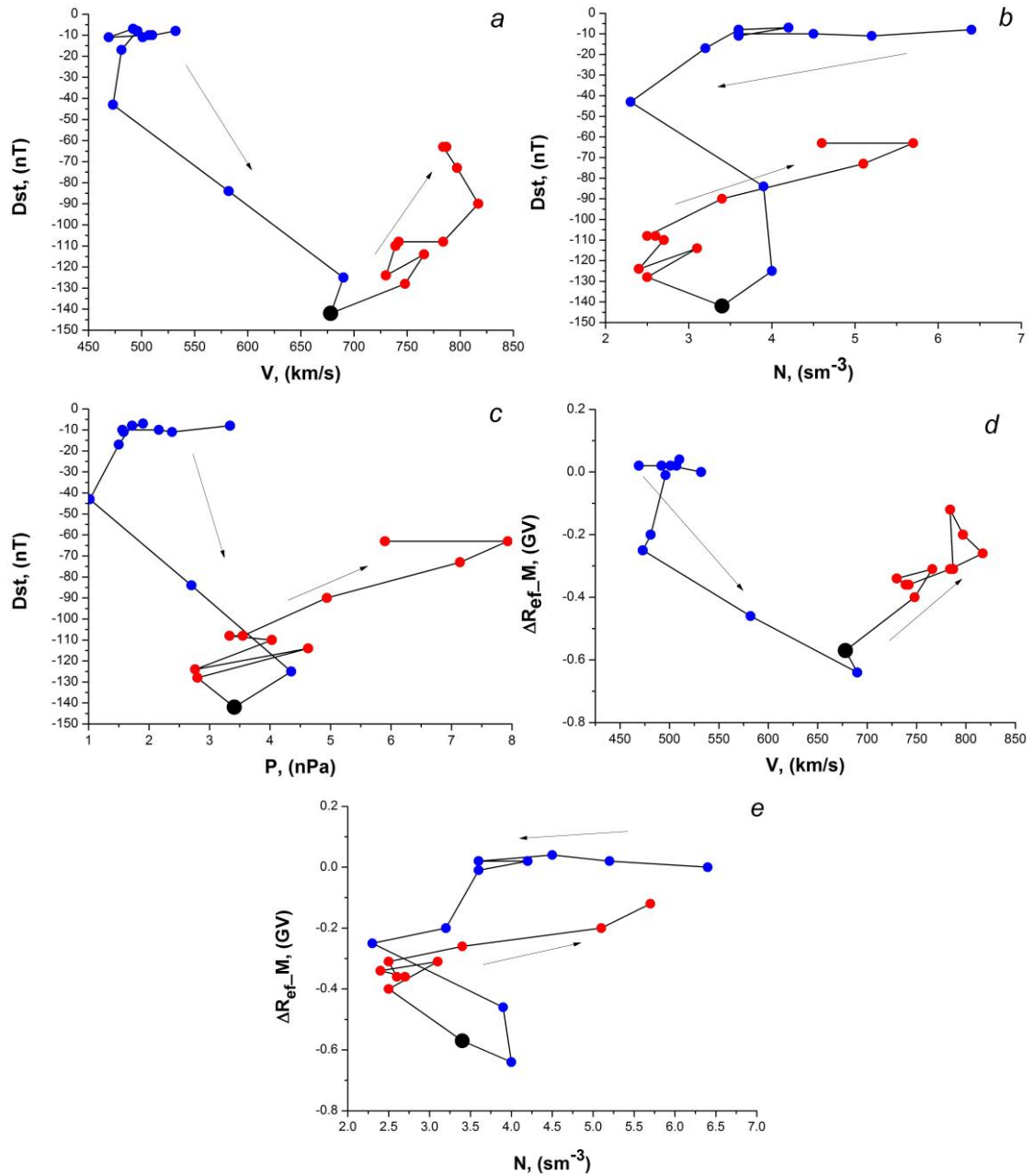

Figure 4. Dependence of *Dst* and variations in the geomagnetic thresholds ΔR_{ef} and ΔR_{sgs} on the SW dynamic parameters *V*, *N*, and *P*. Blue circles mark the main phase; red ones, the recovery phase. Arrows indicate the direction of the lead time of the processes

The dependences of *Dst* and geomagnetic thresholds on the SW dynamic parameters are more complex and less definite in terms of detecting signs of hysteresis. Panels *a–c* demonstrate the ambiguous dependences *Dst*(*V*, *N*, *P*) — a semblance of open hysteresis loops is formed. For the dependence *Dst*(*N* and *P*), a second loop is formed as a response to Dst_{min2}. In panels *d–f*, the dependence of ΔR_{ef} on the SW dynamic parameters virtually repeats *Dst*(*V*, *N*, *P*), showing a similarity to hysteresis. The second loop is clearly seen only for $\Delta R_{\text{ef}}(N)$. Panels *g–i* indicate that the $\Delta R_{\text{sgs}}(V, N, P)$ curves are formed by multiple intersecting lines and produce an analogue of open hysteresis. Thus, the curves of the dependence of *Dst*, ΔR_{ef}, and ΔR_{sgs} on SW dynamic parameters form only a similarity of hysteresis loops, showing less pronounced signs of hysteresis than similar dependences on magnetic and electric parameters.

4. DISCUSSION

Analysis has shown that during the development of the September 7–8, 2017 storm with cyclic variations in SW and IMF parameters hysteresis phenomena occur in the relationship of these parameters with *Dst* and ΔR. The signs of hysteresis are especially obvious for the relationship with the magnetic and electric parameters *B*, B_z, E_y, and β. Our result for the relationship between *Dst* and β supports the conclusions drawn in [Kurazhkovskaya, Kurazhkovsky, 2023], where the presence of hysteresis in the dependence *Dst*(β) on scales of geomagnetic storms has been confirmed. The dependence of geomagnetic thresholds on the SW dynamic parameters is more chaotic, demonstrating only a semblance of hysteresis. This agrees with the results obtained in [Ptitsyna et al., 2021; Danilova et al., 2023], in which it has been shown that during storms in falls of 2003 and 2004 hysteresis loops are most clearly seen for the ΔR dependence on magnetic parameters.

The geomagnetic cutoff rigidity dynamics during the evolution of the storm is a reflection of the interaction of SW and IMF with the geomagnetosphere during this period (see, e.g., [Kichigin et al., 2017; Ptitsyna et al., 2019]. Storm-time activity can be traced by *Dst* variations whose main source for strong storms is the ring current. In the magnetic storm initial phase, field lines of the interplanetary and geomagnetic fields reconnect and dimensions of the magnetosphere fluctuate (they depend on the momentum of the solar plasma stream), which leads to penetration of new particles into the magnetosphere or acceleration of its plasma to energies of the order of thousands of electron volts. During the recovery phase of geomagnetic storms, the ring current decays due to Coulomb scattering and charge exchange of protons with neutral atmospheric hydrogen. At the same time, the times of the ring current saturation and its decay are different [Kozyra, Liemohn, 2003]. It can be assumed that as a result of this the energy is accumulated during the development of the ring current in the storm main phase and is released in the recovery phase asymmetrically, which is a sign of hysteresis. This assumption is supported by the results obtained by Cai et al. [2009]; the authors have simulated the interaction of electromagnetic particles with Earth's magnetosphere. They have shown that with the cyclic variation in $|B_z|$ from 0 to maximum and back when a certain critical value of $|B_z|$ is attained the daytime magnetosphere significantly decreases in size. Hence, the magnetic field is transformed to a form with reduced symmetry in which dissipative processes occur that allow absorbing excess energy coming from SW. Cai et al. [2009] arrive at the conclusion that when the SW energy is transferred to the magnetosphere through dissipative processes, a part of this energy is not restored. At the same time, the restoration of the size and shape of the magnetosphere during the storm recovery phase differs from that during the main phase, thereby forming a hysteresis loop.

The obtained difference between the results for model and observed geomagnetic cutoff rigidities requires separate consideration. Studies based on satellite measurements and model calculations have shown that along with the ring current magnetotail currents can also be an additional source of *Dst* variations [Alexeev et al., 1996; Kalegaev, 2010; Asikainen et al., 2010]. In this case, the ratio between contributions of these current systems depends on the storm strength: very strong storms ($Dst_{\text{min}} < -200$ nT) are derived mainly by the ring current; during less intense disturbances (-200 nT $< Dst_{\text{min}} < -100$ nT), the contribution of tail currents becomes comparable to the contribution of the ring current. The energy stored in the magnetotail, in particular in its more distant part, is responsible for a number of important magnetospheric processes [Borovsky et al., 1998; Ganushkina et al., 2018]. The Ts01 model, we employ to calculate R_{ef}, describes the disturbed magnetic field of the magnetosphere in the region $R \leq 15\ R_E$ and ignores the influence of the field of the middle and distant tail. At the same time, CRs recorded on Earth and employed to determine ΔR_{sgs} are affected by the magnetic field throughout the magnetosphere. Thus, ΔR_{sgs} can reflect the response of CRs to variations in the magnetotail currents better than ΔR_{ef}. The contribution of the tail currents during Dst_{min2} is greater than during Dst_{min1}, so the difference between the responses of ΔR_{ef} and ΔR_{sgs} at this time is more pronounced. If in hysteresis of ΔR_{ef} the second loop as a reaction to the second decrease in *Dst* is only outlined, there are two loops clearly traced in the dependences of ΔR_{sgs} on magnetospheric parameters. Thus, the difference between the obtained hysteresis effects for ΔR_{ef} and ΔR_{sgs} is apparently related to the different sensitivity of the model and observed thresholds to relative contributions of different current systems to *Dst* variations.

CONCLUSION

We have analyzed the complex storm that occurred on September 7–8, 2017 in order to detect possible hysteresis phenomena in the relationship of three paired series: 1) in the dependences of *Dst* on the SW and IMF magnetic and dynamic parameters (*B*, B_z, E_y, β, *V*, *N*, and *P*); 2) in the dependences of model thresholds ΔR_{ef} on the same interplanetary medium parameters; 3) in the

dependences of observed ΔR_{sgs} on the same parameters.

The analysis has revealed for the first time that *Dst* variations depending on IMF and electric field B, B_z, E_y in the main phase of the storm differ from those in the recovery phase — a clear hysteresis loop is formed. Hysteresis loops are also formed for the geomagnetic thresholds ΔR_{ef} and ΔR_{sgs}, calculated by two independent methods. A specific feature of the storm under study is the second decrease in *Dst* during the recovery phase. Hysteresis in the dependence of observed ΔR_{sgs} on magnetospheric parameters better reflects this specific dynamics of the storm. The $\Delta R_{sgs}(B, B_z, E_y, \beta)$ curves form two distinct hysteresis loops as a reaction to two decreases in *Dst*.

In our opinion, hysteresis is explained by the difference between the times of the ring current saturation and its decay. In this case, energy storage during the development of the ring current in the main phase of the storm and its release in the recovery phase occur asymmetrically — hysteresis loops are formed. Other current systems, which develop and decay on different time scales, might have also made an asymmetric contribution to the evolution of the storm. However, the disturbed magnetosphere is a complex multifactor system that is not well understood at present. Additional research is therefore required to draw more specific conclusions about the effect of all components of this system on ΔR.

REFERENCES

Alexeev I.I., Belenkaya E.S., Kalegaev V.V., Feldstein Y.I., Grafe A. Magnetic storms and magnetotail currents. *J. Geophys. Res*. 1996, vol. 101, iss. A4, pp. 7737–7748. DOI: 10.1029/95JA03509.

Asikainen T., Maliniemi V., Mursula K. Modeling the contributions of ring, tail, and magnetopause currents to the corrected *Dst* index. *J. Geophys. Res.: Space Phys*. 2010, vol. 115, iss. A12. DOI: 10.1029/2010JA015774.

Atabekov G.I. *Teoreticheskie osnovy elektrotekhniki. Lineinye elektricheskie tsepi* [Theoretical foundations of electrical engineering. Linear electrical circuits]. Saint Petersburg, Lan Publ., 2009, 592 p. (In Russian).

Borovsky J.E., Thomsen M.F., Elphic R.C., Cayton T.E., McComas D.J. The transport of plasma sheet material from the distant tail to geosynchronous orbit. *J. Geophys. Res*. 1998, vol. 103, iss. A9, pp. 20297–20331. DOI: 10.1029/97JA03144.

Cai D.S., Tao W., Yan X., Lembege B., Nishikawa K.I. Bifurcation and hysteresis of the magnetospheric structure with a varying southward IMF: Field topology and global three-dimensional full particle simulations. *J. Geophys.Res: Space Phys*. 2009, vol. 114, iss. A12210. DOI: 10.1029/2007JA012863.

Danilova O.A., Ptitsyna N.G., Tyasto M.I. Hysteresis phenomena in the relationship between the cosmic ray cutoff rigidity and parameters of the magnetosphere during a storm on May 15, 2005. *Geomagnetism and Aeronomy*. 2023, vol. 63, no. 4, pp. 434–440. DOI: 10.1134/S0016793223600273.

Despirak I.V., Kleimenova N.G., Gromova L.I., Gromov S.V., Malysheva L.M. Supersubstorms during Storms of September 7–8, 2017. *Geomagnetism and Aeronomy*. 2020, vol. 60, no. 3, pp. 292–300. DOI: 10.1134/S0016793220030044.

Dorman L.I., Dorman I.V., Iucci N., Parisi M., Villoresi G. Hysteresis between solar activity and cosmic rays during cycle 22: The role of drifts, and the modulation region. *Adv. Space Res*. 2001, vol. 27, no. 3, pp. 589–594. DOI: 10.1016/S0273-1177(01)00089-8.

Dremukhina L.A., Yermolaev Yu.I., Lodkina I.G. Dynamics of interplanetary parameters and geomagnetic indices during magnetic storms induced by different types of solar wind. *Geomagnetism and Aeronomy*. 2019, vol. 59, iss. 6, pp. 639–650. DOI: 10.1134/s0016793219060069.

Ganushkina N.Y., Liemohn M.W., Dubyagin S. Current systems in the Earth's magnetosphere. *Rev. Geophys*. 2018, vol. 56, pp. 309–332. DOI: 10.1002/2017RG000590.

Gosling J.T. The solar flare myth. *JGR. Space Phys*. 1993, vol. 98, iss. A11, pp. 18937–18949. DOI: 10.1029/93JA01896.

Hajra R, Tsurutani B.T., Lakhina G.S. The complex space weather events of 2017 September. *Astrophys. J*. 2020, vol. 899, no. 1. DOI: 10.3847/1538-4357/aba2c5.

Kalegaev V.V. Dynamic models of the geomagnetic field. *Solnechno-zemnaya fizika* [Solar-Terr. Phys.]. 2010, iss. 16, pp. 60–69. (In Russian).

Kane R.P. Lags, hysteresis, and double peaks between cosmic rays and solar activity. *J. Geophys. Res*. 2003, vol. 108, iss. A10, p. 1379. DOI: 10.1029/2003JA009995.

Kichigin G., Kravtsova M., Sdobnov V. Parameters of current systems in the magnetosphere as derived from observations of cosmic rays during the June 2015 magnetic storm. *Solar-Terr. Phys*. 2017, vol. 3, no. 3, pp. 15–19. DOI: 10.12737/stp-33201702.

Kilpua E.K.J., Balogh A., von Steiger R., Liu Y.D. Geoeffective properties of solar transients and stream interaction regions. *Space Sci. Rev*. 2017, vol. 212, pp. 1271–1314. DOI: 10.1007/s11214-017-0411-3.

Kovalev I.I., Olemskoy S.V., Sdobnov V.E. A proposal to extend the spectrographic global survey method. *J. Atmos. Solar-Terr. Phys*. 2022, vol. 235, p. 105887. DOI: 10.1016/j.jastp.2022.105887.

Kozyra J.U., Liemohn M.W. Ring current energy input and decay. *Space Sci. Rev*. 2003, vol. 109 (1-4), pp. 105–131. DOI: 10.1023/B:SPAC.0000007516.10433.ad.

Kurazhkovskaya N.A., Kurazhkovskii A.Yu. Hysteresis effect between geomagnetic activity indices (Ap, Dst) and interplanetary medium parameter in solar activity cycles. *Solar-Terr. Phys*. 2023, vol. 9, iss. 3, pp. 68–76. DOI: 10.12737/stp-93202308.

Kurazhkovskaya N.A., Zotov O.D., Klain B.I. Relationship between geomagnetic storm development and the solar wind parameter β. *Solar-Terr. Phys*. 2021, vol. 7, no. 4, pp. 25–34. DOI: 10.12737/stp-74202104.

Mavromichalaki H., Belehaki A., Rafios X. Simulated effects at neutron monitor energies: evidence for a 22-year cosmic ray variation. *Astron. Astrophys*. 1998, vol. 330, pp. 764–772.

McCracken K.G., Rao U.R., Shea M.A. The Trajectories of Cosmic Rays in a High Degree Simulation of the Geomagnetic Field. *MIT Tech. Rep. Massachusetts Institute of Technology. Laboratory for Nuclear Science*. Cambridge. 1962. 146 p.

Obridko V.N., Kanonidi K.D., Mitrofanova T.A., Shelting B.D. Solar activity and geomagnetic disturbances. *Geomagnetism and Aeronomy*. 2013, vol. 53, iss. 2, pp. 147–156. DOI: 10.1134/S0016793213010143.

Ptitsyna N.G., Danilova O.A, Tyasto M.I., Sdobnov V.E. Influence of the solar wind and geomagnetic activity parameters on variations in the cosmic ray cutoff rigidity during strong magnetic storms. *Geomagnetism and Aeronomy*. 2019, vol. 59, no. 5, pp. 530–538. DOI: 10.1134/S0016793219050098.

Ptitsyna N.G., Danilova O.A., Tyasto M.I., Sdobnov V.E. Dynamics of cosmic-ray cutoff rigidity and magnetospheric parameters during different phases of the storm of November 20, 2003. *Geomagnetism and Aeronomy*. (Engl. Transl.), 2021, vol. 61, no. 4, pp. 169–179. DOI: 10.1134/S0016793221010114.

Ptitsyna N.G., Danilova O.A., Tyasto M.I., Sdobnov V.E. Cosmic ray cutoff rigidity governing by solar wind and magnetosphere parameters during the 2017 Sep 6–9 solar-terrestrial event. *J. Atmosp. Solar-Terr. Phys*. 2023, vol. 246, p. 106067. DOI: 10.1016/j.jastp.2023.106067.

Richardson I.G., Cane H.V. Geoeffectiveness (*Dst* and K_p) of interplanetary coronal mass ejections during 1995–2009 and implications for storm forecasting. *Space Weather*. 2011, vol. 9, no. 7. DOI: 10.1029/2011sw000670.

Safargaleev V.V., Tereshchenko P.E. Hertz range pulsations during recovery phase of the magnetic storm on September 7–8, 2017, and relation between their dynamics and changes in the parameters of the interplanetary medium. *Geomagnetism and Aeronomy*. 2019, vol. 59, no. 3, pp. 281–295. DOI: 10.1134/S0016793219030125.

Scolini C., Chane E., Temmer M., Kilpua E.K.J., Dissauer K., Veronig A.M., et al. CME-CME interactions as sources of CME geoeffectiveness: the formation of the complex ejecta and intense geomagnetic storm in 2017 early September. *Astrophys. J. Supplement Ser*. 2020, vol. 247 (1). DOI: 10.3847/1538-4365/ab6216.

Serensen S.V., Kogaev V.P., Shneiderovich R.M. *Nesushchaya sposobnost detalei mashin* [Load-bearing capacity of machine parts]. Moscow, Mashinostroenie Publ., 1975, 354 p. (In Russian).

Shen C., Xu M., Wang Y., Chi Y., Luo B. Why the Shock-ICME Complex Structure Is Important: Learning from the Early 2017 September CMEs. *Astrophys. J*. 2018, vol. 861, no. 1, pp. 861–960. DOI: 10.3847/1538-4357/aac204.

Tsyganenko N.A. A model of the near magnetosphere with a dawn-dusk asymmetry: 1. Mathematical structure. *J. Geophys. Res*. 2002a, vol. 107, no. A8, p. 1179. DOI: 10.1029/2001JA000219.

Tsyganenko N.A. A model of the near magnetosphere with a dawn-dusk asymmetry: 2. Parametrization and fitting to observation. *J. Geophys. Res*. 2002b, vol. 107, no. A8, p. 1176. DOI: 10.1029/2001JA000220.

Tsyganenko N.A., Singer H.J., Kasper J.C. Storm-time distortion of the inner magnetosphere: How severe can it get? *J. Geophys. Res*. 2003, vol. 108, no. A5, p. 1209. DOI: 10.1029/2002JA009808.

Yermolaev Yu.I., Lodkina I.G., Nikolaeva N.S., Yermolaev M.Yu. Statistical study of interplanetary condition effect on geomagnetic storms. *Cosmic Res*. 2010, vol. 48, iss. 6, pp. 485–500. DOI: 10.1134/S0010952510060018.

How to cite this article
Danilova O.A., Ptitsyna N.G., Sdobnov V.E. Hysteresis phenomena in the response of geomagnetic activity and cosmic ray parameters to variations in the interplanetary medium during a magnetic storm. *Solar-Terrestrial Physics*. 2024. Vol. 10. Iss. 3. P. 66–74. DOI: 10.12737/stp-103202408.